Experimental Investigation of the Collective Raman Scattering of Multiple Laser Beams in Inhomogeneous Plasmas

S. Depierreux,[1] C. Neuville,[1] C. Baccou,[2] V. Tassin,[1] M. Casanova,[1] P.-E. Masson-Laborde,[1] N. Borisenko,[3] A. Orekhov,[3] A. Colaitis,[4] A. Debayle,[1] G. Duchateau,[4] A. Heron,[5] S. Huller,[5] P. Loiseau,[1] P. Nicolaï,[4] D. Pesme,[5] C. Riconda,[2] G. Tran,[1] R. Bahr,[6] J. Katz,[6] C. Stoeckl,[6] W. Seka,[6] V. Tikhonchuk,[4] and C. Labaune[2]

[1]*CEA, DAM, DIF, F-91297 Arpajon, France*

[2]*LULI, UMR 7605 CNRS, Ecole Polytechnique, 91128 Palaiseau cedex, France*

[3]*P. N. Lebedev Physical Institute, 53 Leninskii Prospect, Moscow 119991 Russia*

[4]*University of Bordeaux-CNRS-CEA, CELIA, F-33405 Talence cedex, France*

[5]*Centre de Physique Théorique, CNRS-Ecole Polytechnique, 91128 Palaiseau cedex, France*

[6]*Laboratory for Laser Energetics, University of Rochester, 250 East River Road, Rochester, New York 14623-1299, USA*

(Received 21 September 2016; revised manuscript received 20 October 2016; published 2 December 2016)

Experiments have been performed evidencing significant stimulated Raman sidescattering (SRS) at large angles from the density gradient. This was achieved in long scale-length high-temperature plasmas in which two beams couple to the same scattered electromagnetic wave further demonstrating for the first time this multiple-beam collective SRS interaction. The collective nature of the coupling and the amplification at large angles from the density gradient increase the global SRS losses and produce light scattered in novel directions out of the planes of incidence of the beams. These findings obtained in plasmas conditions relevant of inertial confinement fusion experiments similarly apply to the more complex geometry of these experiments where anomalously large levels of SRS were measured.

DOI: 10.1103/PhysRevLett.117.235002

A laser electromagnetic wave propagating in an underdense plasma can resonantly couple with the plasma normal modes to give rise to scattered light waves [1–3]. In the case of the coupling with electron plasma waves (EPW), the instability is called stimulated Raman scattering (SRS) and produces light scattered with wavelengths up to twice the one of the incident laser. Anomalously high SRS losses that significantly undermine the target performance were measured, sometimes in unforeseen directions, in the large number of beams inertial confinement fusion (ICF) [4] experiments performed at the megajoule energy level [5–10]. While the instabilities of one individual laser beam in a homogeneous plasma are expected to mainly develop along the beam propagation axis, the interaction of multiple beams in an inhomogeneous plasma as occurs in ICF experiments involves intricate physical mechanisms that may result in increased amplification of the scattered light in new directions.

In configurations involving multiple beams, collective instabilities could develop that modify the preferential decay geometry [11]. These collective instabilities can occur in the case of laser beams having a common symmetry axis along which they drive a common daughter wave. It was evidenced in experiments for the two plasmon decay instability [12–14] and for the stimulated Brillouin scattering [15]. This type of collective instability for SRS is expected to result in increased SRS amplification at various angles by sidescattering of the multiple beams. The growth of SRS for a single beam may also produce significant sidescattering in an inhomogeneous plasma in the geometries where the scattered light is amplified along directions close to the normal to the density gradient [16–17] where the effective plasma inhomogeneity is strongly reduced. This redshifted SRS scattered light, emitted at large oblique angles from the density gradient, is however expected to experience significant collisional absorption and refraction before exiting the plasma making it difficult to observe in experiments.

We have taken advantage of the collective amplification of such an SRS sidescattered wave by multiple beams to evidence this process at large angles from the density gradient in experiments performed in high-temperature, low-Z, long scalelength plasmas. The experiment described in this Letter is also the first that demonstrates this multiple-beam collective SRS interaction with a common sidescattered wave. Two cones of six beams were incident on both sides of a low-density foam target at 60° with respect to the target normal. The angular distribution of the SRS scattered light, measured around the bisecting plane of two beams, evidences a significant signal corresponding to the collective SRS of the two beams sharing a scattered electromagnetic wave. The signal maximized at an angle of ∼48° from the target normal where the corresponding time-resolved spectrum was also measured. This observation in vacuum corresponds to SRS light produced at ∼80° from the density gradient in the plasma region of interaction. This optimum angle results from the increase of the SRS collective gain partly compensated by the increased

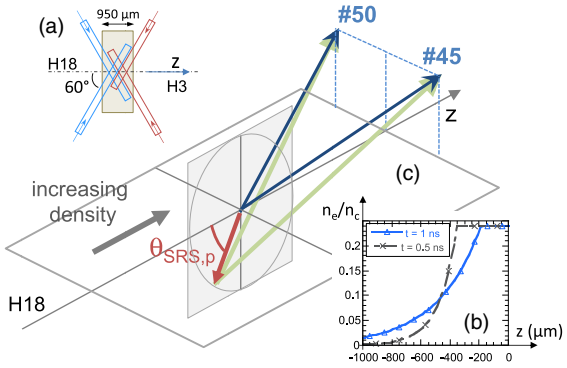

FIG. 1. (a) Schematic representation of the two cones of beams in the foam target; (b) density profile along the z axis at $t = 0.5$ and 1 ns; (c) 3D representation of the sidescattering geometry in the bisecting plane of beams 45 and 50. The conjugate EPWs in this collective excitation are represented by the green arrows for beams 45 and 50.

collisional absorption of the SRS signal as the light is scattered at larger angles from the density gradient. The collective nature of the coupling and the amplification at large angles from the density gradient are found to increase the global SRS losses and to produce light scattered outside the planes of incidence of the two beams in directions that we characterize experimentally.

The experiments were performed on the 351 nm Omega laser facility at the University of Rochester. The targets were 7 mg/cc $C_{12}H_{16}O_8$ foams [18] with a diameter of 2.5 mm and a length of 950 μm aligned along the H3-H18 axis of the Omega target chamber. The laser beams were focused by $f/6.7$ lenses through elliptical phase plates producing spot sizes with a 200×300 μm diameter (full width at half maximum). These beams were fired at the energy level of 400 J in a 1 ns square pulse producing a maximum intensity of 7×10^{14} W/cm^2 per beam. This intensity was chosen to produce a supersonic ionization of the low density foam. Previous experiments [19–23] performed with similar foams and analytical modeling [24] indicate that the ionization front propagates at a speed of 0.9 mm/ns in a 7 mg/cc foam. Twelve beams were used, incident at 60° from the foam axis, making a 6-beams cone on each side of the target. Figure 1(a) represents a side view of the geometry of these beams in the target. On each side, the beams were shifted from the center of the target by 150 μm, measured along the foam axis [z axis in Fig. 1(a)], towards the foam entrance. After ~0.5 ns, the regions of foam ionized by the different beams of a same cone start superimposing. After this time, the remaining foam is rapidly ionized and heated.

During the ionization of the foam target, the plasma expands along the z axis over the surface ($\varnothing \sim 1.3$ mm) covered by the cone of 60° beams. For the times of interest ($t = 0.5$–1 ns), this expanding plasma presents an exponential density profile along z with a characteristic length $L_n \sim c_s\, t \sim 300$ μm at $t = 1$ ns. This expansion can be considered as monodimensional for the times of interest ($t < 1$ ns) for which the plasma scale length is still small compared to the transverse size of the irradiated zone $\varnothing \gg L_n$. Exponential density profiles are used to fit the results of hydrodynamics simulations with a good accuracy. These density profiles are shown in Fig. 1(b) for $t = 0.5$ and 1 ns. The electron temperature was measured with thermal Thomson scattering [25] validating the electron temperature ($T_e \geq 2$ keV) found in the hydrodynamics simulations at $t = 1$ ns.

The angular distribution of the 6 beams incident on the H18 side is schematically shown in Fig. 2(a) together with the representation of the near backscattered imager (NBI) that measured the time-integrated angular distribution of the light scattered in the Raman wavelength range $\lambda_{SRS} = [450–900]$ nm. This diagnostic collects the SRS light scattered around the midplane [see Fig. 1(c)] of beams 45 and 50 with angles between 20° and 60° from the target normal. A typical image recorded on this diagnostic is shown in Fig. 2(b). The SRS scattered light is observed at angles of ±6° around the midplane close to the region mentioned as FABS25 located at ~48° from the z axis. The time-resolved spectrum of the light scattered in this direction collected in an aperture of ±4° was also measured with temporal and spectral resolutions of 100 ps and 9 nm. The corresponding SRS spectrum is shown in Fig. 2(c). The SRS signal starts at $t \sim 0.5$ ns, as soon as the beams start overlapping in the foam plasma. It lasts until the end of the laser pulses with an almost constant wavelength of $\lambda_{SRS} \sim 600$ nm. Absolute energy measurements performed in a calorimeter in this same direction indicate that the SRS losses associated with this signal maximize at ~5% of the power available in one beam. Shots were performed with foams of different densities with beams fired at slightly

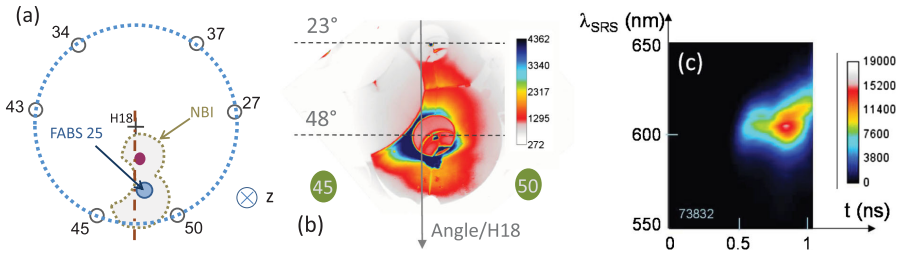

FIG. 2. (a) Angular distribution of the 6 beams incident on the H18 side and scheme of the NBI diffuser plate; (b) typical image recorded with the NBI diagnostic for a 7 mg/cc foam; (c) time-resolved spectrum of the SRS light collected in the direction of FABS25 in the same shot as for (b).

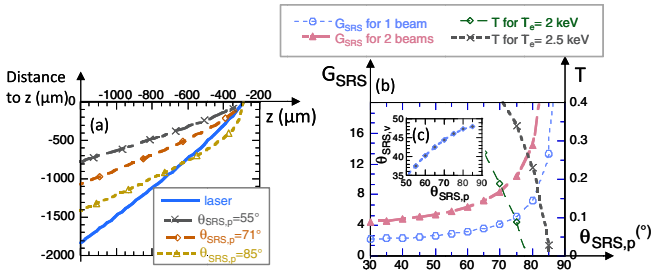

FIG. 3. (a) calculated refraction of the 351 nm laser light and of 600 nm SRS light for $\theta_{\mathrm{SRS},p} = 55°$, 71°, and 85° in the density profile for $t = 1$ ns; (b) Rosenbluth gain (G_{SRS}) for $n_e/n_c = 0.17$ as a function of $\theta_{\mathrm{SRS},p}$ and transmission (T) of the SRS light for $\lambda_{\mathrm{SRS}} = 600$ nm through the density profile at $t = 1$ ns. G_{SRS} is calculated for 2 beams with polarizations aligned with the scattered light; (c) exit angle ($\theta_{\mathrm{SRS},v}$) of the SRS light produced at $n_e/n_c = 0.17$ as a function of $\theta_{\mathrm{SRS},p}$.

different energy levels and the signal measured in the three diagnostics all varied in proportion confirming their common origin.

As would be expected for a two-beam collective SRS instability, the scattered light is maximum in the bisecting plane of the two beams. However, a collective scattering involving only two beams could develop over a range of sidescattering angles in this plane. Rather, in the experiment, the SRS scattered light is observed to be concentrated at angles between 42° and 54° measured with respect to the target normal. These experimental observations are, however, perfectly consistent with the amplification of a collective SRS instability in the inhomogeneous plasma by the two neighboring beams (beams 45 and 50) in their region of overlap. We first take into account the propagation of the 351 nm light on its way inside the plasma. The latter is refracted as it propagates to higher densities so that the laser beams cross the original foam axis in $z < -150$ μm. The laser beam path is illustrated in Fig. 3(a) for $t = 1$ ns. The two beams cross in $z = -300$ μm where the electronic density is $0.17\,n_c$ in agreement with the measured value for their SRS signal of $\lambda_{\mathrm{SRS}} \sim 600$ nm. In the region of beam crossing, the 351 nm light makes an angle of ~71° with the density gradient. The absorption of the 351 nm light before it reaches this region is negligible.

We next consider the SRS sidescattering of the two beams in their bisecting plane represented by the red dashed-dotted vertical line in Fig. 2(a). In the following, the geometry of this SRS sidescattering for beams 45 and 50 will be specified through the angle, $\theta_{\mathrm{SRS},p}$, measured in their bisecting plane, between the sidescattered light and the z axis [see Fig. 1(c)]. The density gradient in the region of beams overlap is approximated by a linear ramp with a characteristic scale length $L_n = 300$ μm. The Rosenbluth SRS gain factor in amplitude [26] for the amplification of the SRS light as a function of $\theta_{\mathrm{SRS},p}$ is shown in Fig. 3(b). This calculation [16–17] takes into account the oblique incidence of the 351 nm light, the Raman decay sidescattering geometry and the inhomogeneity. The Rosenbluth gain factor increases like $L_n/\cos(\theta_{\mathrm{SRS},p})$ that provides the main dependence. This formula remains valid until the WKB approximation made to calculate the Rosenbluth gain fails. In long scale-length plasmas, this occurs in the close vicinity of $\theta_{\mathrm{SRS},p} = 90°$ only (for $\theta_{\mathrm{SRS},p} > 88°$ for the parameters of this experiment).

The increase of the SRS gain with $\theta_{\mathrm{SRS},p}$ is counterbalanced by the absorption of the SRS light on its way outside the plasma when it is emitted at larger $\theta_{\mathrm{SRS},p}$. The paths of the SRS light in the plasma is shown for three values of $\theta_{\mathrm{SRS},p}$ in Fig. 3(a). As $\theta_{\mathrm{SRS},p}$ increases, the SRS light must travel through longer plasma regions before exiting so that it experiences more collisional absorption. The amount of SRS light transmitted through the plasma is also shown in Fig. 3(b) as a function of $\theta_{\mathrm{SRS},p}$. For angles larger than 85°, the SRS light is fully absorbed in the plasma so that one would expect that even if this instability develops, the corresponding SRS light would not be observable in experiments. The product $T \times \exp(G_{\mathrm{SRS}})$ maximizes for $\theta_{\mathrm{SRS},p} \sim 75°$–80° which is consequently the expected optimum angle for the observation of the collective SRS of beams 45 and 50. For this angle, significant amplification of the SRS light is expected from the calculated Rosenbluth gain ($G_{\mathrm{SRS}} > 10$) and 10%–30% of the SRS light is transmitted. Taking into account the refraction of this SRS light as illustrated in Fig. 3(c) gives an angle of ~47° for its observation in vacuum in good agreement with the experiment.

A striking feature in the data recorded in FABS25 is the small range of wavelengths covered by the SRS signals when the conditions were changed. The spectra measured for foams with 4, 5, and 7 mg/cc are compared in Fig. 4(a) showing that the SRS signal remains confined between $\lambda_{\mathrm{SRS}} = 570$ nm and $\lambda_{\mathrm{SRS}} = 620$ nm. Figure 4(b) illustrates the refraction of the SRS light as a function of its wavelength for various angles of production, $\theta_{\mathrm{SRS},p}$, in the plasma around the optimum. Since FABS25 collects the SRS light refracted with $\theta_{\mathrm{SRS},v}$ between 44° and 52°, Fig. 4(b) explains the small extent in λ_{SRS} observed in the measured spectra. Also, the short wavelength cutoff observed at $\lambda_{\mathrm{SRS}} = 570$ nm tends to indicate that little SRS amplification is possible for $\theta_{\mathrm{SRS},p} < 75°$. Figure 4(b) similarly explains the small extent in $\theta_{\mathrm{SRS},v}$ (between 42° and 54°) observed in the NBI diagnostic. Considering the finite size of the two beams and their geometry, we illustrate, in Figs. 4(c) and 4(d), their overlap in two planes perpendicular to the z axis and located in $z = -300$ μm and $z = -350$ μm. This analysis indicates that the collective SRS signal could be amplified by the two beams in the 7 mg/cc foam plasma for electronic densities ranging approximately from $n_e/n_c = 0.14$ (or

$\lambda_{SRS} = 589$ nm) to $n_e/n_c = 0.195$ (or $\lambda_{SRS} = 651$ nm). In this range, the expected $\theta_{SRS,v}$ nearly decreases from 52° down to 35° for $\theta_{SRS,p} > 75°$. The large angle cutoff is close to the experimental observations but very little light can be detected in the NBI diagnostic for $\theta_{SRS,v} < 42°$. In the corresponding longest wavelengths range, the SRS light is produced at larger densities preventing its detection outside the plasma.

This analysis is further confirmed by the shots performed in lower density foams (5 mg/cc) at the slightly reduced beam energy of 350 J. The SRS signal, shown in Fig. 4(a), was reduced by a factor of ~3 compared to the higher energy, 7 mg/cc measurements. This experiment was repeated with beams 45 and 50 pointed in the middle of the foam rather than in $z = -150$ μm. With this new pointing, the beams cross each other in a denser plasma with n_e/n_c up to 0.24. The signals measured in the FABS25 and NBI were reduced by a factor ~10 compared to what was observed with the original pointing. This confirms that either the SRS collective signal could not grow for these higher densities or that its absorption in these denser regions prevents its observation outside the plasma. In these conditions where the collective SRS signature outside the plasma was strongly reduced, we have been able to detect the lowest single beam sidescattered SRS signal of beam 50 in the NBI diagnostic. The latter remains located close to the original aperture of beam 50 (up to sidecattering angles of ~5° compared to the original beam aperture) and is ~10 times lower than the collective SRS signal measured with the beams pointed in $z = -150$ μm. This confirms that the individual beam sidescattering contribution in the signal previously discussed is negligible.

A level of ~5% of collective SRS sidescattering has been measured representing only a fraction of the global SRS light which is mostly absorbed before exiting the plasma. The hot electrons simultaneously generated by the driven EPW are also of primary concern in the ICF context [27]. For the parameters of this experiment, $n_e = 0.17\, n_c$ and for $\theta_{SRS,p} \sim 75$–80°, the trapping of electrons in the stimulated EPW is expected to accelerate hot electrons with energies ~25 keV. In this experiment, the hot electron component was inferred from the hard x-ray emission it produces via bremsstrahlung in the foam plasma [28]. The Hard X-ray Detector [29] gives an electron temperature of ~20 keV close to the expected value. According to recent calibrations [30], significant levels of x-ray signals were measured in this experiment. The corresponding total energy invested in these hot electrons depends on the details of the x-ray emission. However, from simple models [28], we estimate that this energy is of at least a few hundreds joules consistent with losses of more than 10% of the laser beams power. These hot electrons propagate inward along the driven EPW shown by the green arrows in Fig. 1(c).

The plasma conditions reached in our experiment, i.e., an exponential density profile with $L_n \sim 300$ μm and $T_e \sim 2$ keV, approach those of megajoule scale direct-drive experiments [31,32]: $L_n \sim 350$–600 μm, $T_e \sim 3.5$–5 keV and laser intensities $I = 4$–10×10^{14} W/cm^2. The mechanism evidenced in our experiment is so expected to similarly develop in these experiments. It could occur between any pair of beams over a broad range of electronic density to produce SRS light in the bisecting plane of the two beams almost transverse to the target normal that is further refracted and absorbed before exiting the plasma. The resulting angular distribution of this SRS light then depends on the specific geometry of each experiment. Because this SRS is refracted and absorbed in the plasma, its diagnostic will remain very partial in most of the experiments making it difficult to accurately estimate the associated losses. Inhomogeneous density profiles are also present in the region of crossing beams at the laser entrance hole early in the laser pulse in indirect-drive configurations [33,34]. In these experiments, performed with a large number of beams, this pairwise coupling is expected to accelerate hot electrons all propagating forward with directions that depend on the detailed geometry of the beams and energies that increase with the SRS sidescattering angle.

The large amplification of SRS electromagnetic waves almost transverse to the density gradient as theoretically

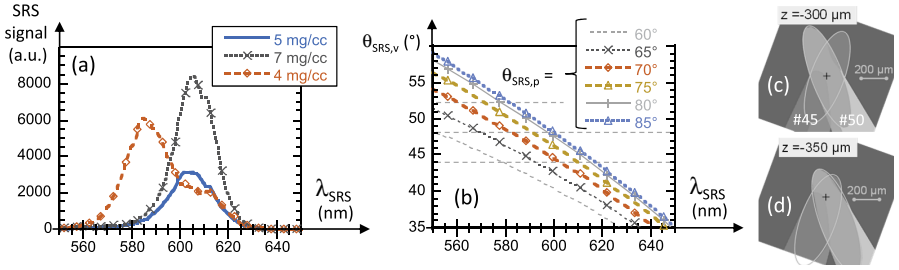

FIG. 4. (a) SRS spectra measured in FABS25 for different conditions: in 4 mg/cc and 7 mg/cc foams at 400 J and in a 5 mg/cc foam at 350 J; (b) exit angle of the SRS light for the various densities in the crossing beams region shown as a function of its wavelength; the gray dashed lines represent the aperture of FABS25; representation of the two beams overlay in the planes (c) $z = -300$ μm and (d) $z = -350$ μm. The laser beam spots are shown for two beams incident at 71° of the z axis and overlapping in $z = -300$ μm. The contours are shown at 50% of the maximum intensity.

predicted 40 years ago has been evidenced in hot long scale-length plasmas. The occurrence of the collective Raman scattering instability in which multiple beams couple to the same scattered light wave has been demonstrated for the first time. This mechanism was successfully invoked to explain the large level of SRS measured in indirect-drive ICF [6,35]. The collective coupling and the amplification at large angle from the density gradient increase the amount of SRS losses that are only partly measured in experiments due to the refraction and absorption of the redshifted SRS light. Depending on the beams' geometry, mitigation strategies may have to be developed like reducing spot sizes which will push the beams' overlay to denser plasma regions where SRS could not grow.

The experiment described in this manuscript was funded by the Agence Nationale pour la Recherche under the ANR project ILPHYGERIE (ANR-12-BS04-0006-01). We gratefully acknowledge the Omega operating teams.

[1] J. F. Drake, P. K. Kaw, Y. C. Lee, G. Schmidt, C. S. Liu, and M. N. Rosenbluth, Parametric instabilities of electromagnetic waves in plasmas, Phys. Fluids **17**, 778 (1974).

[2] D. W. Forslund, J. M. Kindel, and E. L. Lindman, Theory of stimulated scattering processes in laser-irradiated plasmas, Phys. Fluids **18**, 1002 (1975).

[3] W. L. Kruer, *The Physics of Laser Plasma Interactions* (Addison-Wesley, Redwood City, CA, 1988).

[4] J. D. Lindl, Development of the indirect-drive approach to inertial confinement fusion and the target physics for ignition and gain, Phys. Plasmas **2**, 3933 (1995).

[5] N. B. Meezan *et al.*, National Ignition Campaign Hohlraum energetics, Phys. Plasmas **17**, 056304 (2010).

[6] D. E. Hinkel *et al.*, Stimulated Raman scatter analyses of experiments conducted at the National Ignition Facility, Phys. Plasmas **18**, 056312 (2011).

[7] M. J. Rosenberg *et al.*, Planar laser-plasma interaction experiments at direct-drive ignition-relevant scale lengths at the national ignition facility, Bull. Am. Phys. Soc. **61**, 231 (2016).

[8] W. Seka, M. J. Rosenberg, W. Theobald, J. F. Myatt, A. V. Maximov, R. W. Short, S. P. Regan, P. A. Michel, C. Goyon, and J. D. Moody, Stimulated Raman scattering in direct-drive inertial confinement fusion plasmas, Bull. Am. Phys. Soc. **61**, 388 (2016).

[9] P. Michel *et al.*, SRS analyses of direct-drive ICF experiments at National Ignition Facility, Bull. Am. Phys. Soc. **61**, 388 (2016).

[10] A. A. Solodov *et al.*, Modeling laser-plasma interactions at direct-drive ignition-relevant plasma conditions at the National Ignition Facility, Bull. Am. Phys. Soc. **61**, 388 (2016).

[11] D. F. DuBois, B. Bezzerides, and H. A. Rose, Collective parametric instabilities of many overlapping laser beams with finite bandwidth, Phys. Fluids **B4**, 241 (1992).

[12] C. Stoeckl *et al.*, Multibeam Effects on Fast-Electron Generation from Two-Plasmon-Decay Instability, Phys. Rev. Lett. **90**, 235002 (2003).

[13] D. T. Michel, A. V. Maximov, R. W. Short, S. X. Hu, J. F. Myatt, W. Seka, A. A. Solodov, B. Yaakobi, and D. H. Froula, Experimental Validation of the Two-Plasmon-Decay Common-Wave Process, Phys. Rev. Lett. **109**, 155007 (2012).

[14] R. K. Follett, D. H. Edgell, R. J. Henchen, S. X. Hu, J. Katz, D. T. Michel, J. F. Myatt, J. Shaw, and D. H. Froula, Direct observation of the two-plasmon-decay common plasma wave using ultraviolet Thomson scattering, Phys. Rev. E **91**, 031104(R) (2015).

[15] C. Neuville *et al.*, Experimental Evidence of the Collective Brillouin Scattering of Multiple Laser Beams Sharing Acoustic Waves, Phys. Rev. Lett. **116**, 235002 (2016).

[16] C. S. Liu, M. N. Rosenbluth, and R. B. White, Raman, and Brillouin scattering of electromagnetic waves in inhomogeneous plasmas, Phys. Fluids **17**, 1211 (1974).

[17] B. B. Afeyan and E. A. Williams, Stimulated Raman sidescattering with the effects of oblique incidence, Phys. Fluids **28**, 3397 (1985).

[18] A. M. Khalenkov, N. G. Borisenko, V. N. Kondrashov, Y. A. Merkuliev, J. Limpouch, and V. G. Pimenov, Experience of micro-heterogeneous target fabrication to study energy transport in plasma near critical density, Laser Part. Beams **24**, 283 (2006).

[19] S. Depierreux *et al.*, Laser Smoothing and Imprint Reduction with a Foam Layer in the Multikilojoule Regime, Phys. Rev. Lett. **102**, 195005 (2009).

[20] Ph. Nicolaï *et al.*, Experimental evidence of foam homogenization, Phys. Plasmas **19**, 113105 (2012).

[21] C. Goyon, S. Depierreux, V. Yahia, G. Loisel, C. Baccou, C. Courvoisier, N. G. Borisenko, A. Orekhov, O. Rosmej, and C. Labaune, Experimental Approach to Interaction Physics Challenges of the Shock Ignition Scheme Using Short Pulse Lasers, Phys. Rev. Lett. **111**, 235006 (2013).

[22] S. Depierreux, V. Yahia, C. Goyon, G. Loisel, P.-E. Masson-Laborde, N. Borisenko, A. Orekhov, O. Rosmej, T. Rienecker, and C. Labaune, Laser light triggers increased Raman amplification in the regime of nonlinear Landau damping, Nat. Commun. **5**, 4158 (2014).

[23] V. Yahia *et al.*, Reduction of stimulated Brillouin backscattering with plasma beam smoothing, Phys. Plasmas **22**, 042707 (2015).

[24] S. Yu Gus'kov, J. Limpouch, Ph. Nicolaï, and V. T. Tikhonchuk, Laser-supported ionization wave in underdense gases and foams, Phys. Plasmas **18**, 103114 (2011).

[25] J. Katz, R. Boni, C. Sorce, R. Follett, M. J. Shoup III, and D. H. Froula, A reflective optical transport system for ultraviolet Thomson scattering from electron plasma waves on Omega, Rev. Sci. Instrum. **83**, 10E349 (2012).

[26] M. N. Rosenbluth, Parametric Instabilities in Inhomogeneous Media, Phys. Rev. Lett. **29**, 565 (1972).

[27] R. P. Drake, R. E. Turner, B. F. Lasinski, K. G. Estabrook, E. M. Campbell, C. L. Wang, D. W. Phillion, E. A. Williams, and W. L. Kruer, Efficient Raman Sidescatter and Hot-Electron Production in Laser-Plasma Interaction Experiments, Phys. Rev. Lett. **53**, 1739 (1984).

[28] W. C. Mead *et al.*, Laser irradiation of disk targets at 0.53 μm wavelength, Phys. Fluids **26**, 2316 (1983).

[29] C. Stoeckl, V. Yu. Glebov, D. D. Meyerhofer, W. Seka, B. Yaakobi, R. P. J. Town, and J. D. Zuegel, Hard x-ray detectors for Omega and NIF, Rev. Sci. Instrum. **72**, 1197 (2001).

[30] C. Stoeckl, W. Theobald, S. P. Regan, and M. H. Romanofsky, Calibration of a time-resolved hard x-ray detector using radioactive sources, Rev. Sci. Instrum. **87**, 11E323 (2016).

[31] A. A. Solodov *et al.*, Hydrodynamic simulations of long-scale-length plasmas for two-plasmon-decay planar-target experiments on the NIF, J. Phys. Conf. Ser. **717**, 012053 (2016).

[32] M. Hohenberger *et al.*, Polar-direct-drive experiments on the National Ignition Facility, Phys. Plasmas **22**, 056308 (2015).

[33] P. Michel, L. Divol, E. L. Dewald, J. L. Milovich, M. Hohenberger, O. S. Jones, L. Berzak Hopkins, R. L. Berger, W. L. Kruer, and J. D. Moody, Multibeam Stimulated Raman Scattering in Inertial Confinement Fusion Conditions, Phys. Rev. Lett. **115**, 055003 (2015).

[34] E. L. Dewald *et al.*, Generation and Beaming of Early Hot Electrons onto the Capsule in Laser-Driven Ignition Hohlraums, Phys. Rev. Lett. **116**, 075003 (2016).

[35] J. F. Myatt *et al.*, Multiple-beam laser-plasma interactions in inertial confinement fusion, Phys. Plasmas **21**, 055501 (2014).